Journal of Materials Chemistry A

Accepted Manuscript

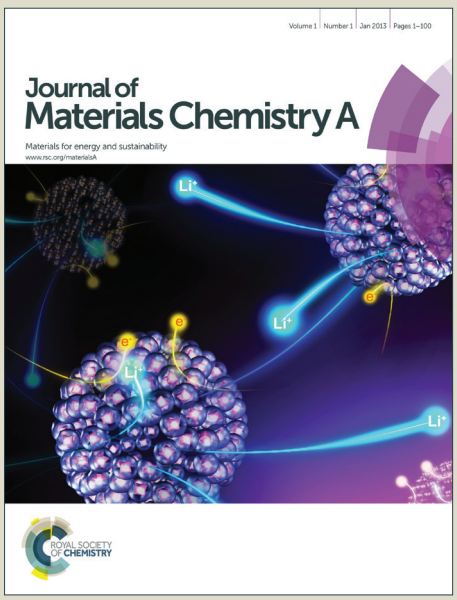

ROYAL SOCIETY OF CHEMISTRY

www.rsc.org/materialsA

Journal of Materials Chemistry A

Journal of Materials Chemistry A

Dynamic Article Links ►

Cite this: DOI: 10.1039/c0xx00000x

ARTICLE TYPE

www.rsc.org/xxxxxx

Morphology of latex and nanocomposite adsorbents prepared by freeze-casting

Lucimara Lopes da Silva,[a] and Fernando Galembeck*[a,b]

Received (in XXX, XXX) Xth XXXXXXXXX 20XX, Accepted Xth XXXXXXXXX 20XX

DOI: 10.1039/b000000x

Freeze-casting liquid dispersions of solid particles is a useful alternative for making porous solids, thus creating lightweight and mechanically resistant materials for various applications. This work describes and discusses the different morphologies obtained by freeze-casting poly(styrene-acrylic) latex aqueous dispersions, either pristine or foamed and comparing them to those prepared following addition of nanoclay. Surface area and dye sorption capacity of freeze-cast latex/clay nanocomposite monoliths are much higher than those of freeze-cast latex only and pore morphology is also different in these solids. Freeze-cast polymer displays an interesting morphology including a fishbone shape unprecedented in non-crystalline solids cast from aqueous media. Quite different, latex-clay nanocomposite exhibits only lamellar pores with irregular features on their walls. These differences are assigned to the stiffening role of the clay lamellae on the rubbery polymer, reducing the extent of particle aggregation and coalescence and thus preserving voids. Dispersion foaming prior to freeze-casting produces additional features in the solids but without making a positive contribution to surface area and dye sorption capacity. These results are understood considering pore templating by ice crystal growth and the templating effect of clay particles on fine ice morphology.

Introduction

Currently, the efficient removal of dyes from wastewaters is essential since their discharge in water bodies is strictly prohibited worldwide and affects both aquatic life and water quality.[1] Commonly used methods for dye removal include adsorption, photocatalysis, dye coagulation/flocculation, membrane filtration, photodegradation and biodegradation. Among these, adsorption is widely used due to its low cost, high efficiency and simplicity.[2]

Several porous materials have been employed as absorbents such as activated carbon and carbon nanotubes,[3] clays,[2] hybrid aerogels,[4] natural and synthetic polymers and their composites.[5-7] Polymer materials are used to design structured porous and surface morphology and are found in a wide range of applications, from tissue engineering[8] to automotive parts and process intensification.[9]

A great variety of methods have been utilized to obtain porous and/or aligned materials including gel casting,[10] gas bubbling,[11] dense gas foaming,[12] spray-drying,[13] electrospray,[14] electrospinning,[8] layer-by-layer[15] and eutectic growth[16] but freeze-casting process is simple and environmentally friendly.[17]

The freeze-casting process, based on the lyophilization of a frozen suspension within a mold, enables the formation of porous structures which replicate ice crystals formed under steep temperature gradients resulting in materials with oriented pores.[18-21] This produces singular permeation properties coupled to high specific surface area, in addition to mechanical strenghtening in a specific direction due to the anisotropic pore structure.[19-22] Moreover, several factors can be used to control pore size, as the use of additives,[17] the solidification rate, the use of different solvents and polymers[23] and solids content of the initial suspension.[18,23,24]

Because of its versatility, freeze-casting has been applied to a wide range of materials from polymers to ceramic suspensions,[17,25-27] metals and their composites[28] targeting mechanically resistant[18,29] and/or absorbent /adsorbent lightweight materials.[30-32] However, reports about freeze-casting use in order to shape structured adsorbents are sparse and focus solely on the use of zeolites.[31,32] Similarly, there are few reports on polymer with clay nanocomposites made by freeze-casting, targeted for strengthening ceramics.[17,25,27]

Layered silicates (clays) as sodium montmorillonite are easily available and have been widely used in polymer matrices to improve thermal, mechanical and solvent resistance of nanocomposites.[33] Further, clays are used to adsorb water soluble pigments and dyes from major sources of environmental pollution (textiles, printing, dyeing, etc).[34]

Gawryla and Schiraldi[30] used different water-soluble synthetic polymers (poly(vinyl alcohol), poly(acrylic acid), poly(ethylene oxide) and poly(ethylene glycol)) to improve the mechanical strength of sodium montmorillonite aerogels,[35] with densities

typically from 0.01 to 0.1 g cm^{-3}. They obtained freeze-cast lightweight highly absorbent nanocomposite aerogels. These aerogels have lamellar structure resulting from alignment of clay particles along the ice crystal faces,[30,35] which opens the possibility to obtain nanocomposites with good compressive strength, since clay lamellae can orient forming columns.

Beyond the polymer materials mentioned above, latex was used only to produce natural rubber latex (NR) nanocomposites with a range of clay contents by freeze-casting.[29,36-38] In these cases, clay contributed a regular layered morphology.

The present work also describes freeze-cast clay-polymer nanocomposites but using a latex with T_g in the room-temperature range and thus much higher than natural rubber.[39] Morphologies templated by ice are thus preserved at room temperature.

Experimental section

Materials

Sodium montmorillonite (NaMMT) was acquired from Southern Clay Products (cation exchange capacity = 102 mequiv/100 g clay). Methylene blue (MB) dye was from Synth. Poly(styrene-butyl acrylate-acrylic acid) latex (P(S-BA-AA)), with 32% dry weight, T_g = 51±1 °C, 55 nm particle diameter (ø) and –10±2 mV zeta potential (ζ), was prepared in this laboratory according to Keslarek et al.[40] Other samples of styrene-acrylate were poly(styrene-butyl acrylate) (P(S-BA)) commercial resins, Acronal 295 D (53% dry weight, T_g = 25 ±1 °C, ø = 100 nm, ζ= –80±2 mV) and Denvercril RA 193 (51% dry weight, TMFF = 18 °C, ø = 55 nm, ζ= –11±2 mV), supplied by BASF (São Paulo, Brazil) and Denver (São Paulo, Brazil), respectively. Milli-Q deionized water was used throughout.

Composite preparation

NaMMT was dispersed in water with continuous stirring using a blade propeller at 1000 rpm for 24 h to yield a 2.65 % w/w clay dispersion. The nanocomposite containing 6% clay (relative to total solids in dry samples) was prepared by mixing 7.7 g clay dispersion to 10 g latex. The mixture was slowly homogenized for 10 min at room temperature, using a magnetic stirrer to yield an aqueous precursor dispersion containing 1.15 % w/w clay. Latex and nanocomposite were also foamed using a blade propeller at 1500 rpm for 10 minutes, yielding samples with about twice the volume of the liquid samples. Each suspension (1.0 mL) was transferred to cylindrical glass molds (4.0 cm length, ø = 1.1 cm), immediately dipped into liquid nitrogen and kept for 10 minutes (although freezing time was only 1 minute). The bottom of the molds contacted liquid nitrogen first, in order to provoke unidirectional freezing. The molds were placed within 250 mL round bottom glass flasks previously cooled by immersion in liquid nitrogen and subsequently mounted on a home-made freeze-drying apparatus (described in the Supplementary Information, Fig. S1), operating at 90 mmHg for 6 hours.

Larger monoliths required for apparent density determination and compression tests were prepared by pouring 20.0 mL of each suspension into ø= 50mm glass Petri dishes, frozen in the same way and freeze-dried (freeze-dryer Terroni, model LB 300 TT (São Carlos, SP)) at low pressure (0.001 mmHg) for 24 hours. For the sake of comparison, the latex and its nanocomposite were air-dried at 60 °C. Schematic illustration of experimental steps for sample preparation is in Fig. 1.

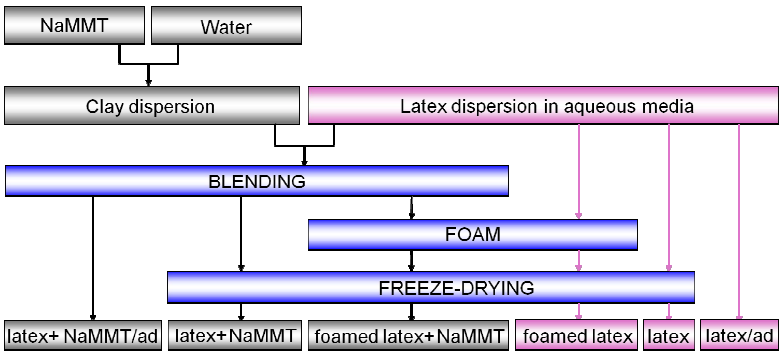

Fig. 1. Preparation of freeze-cast and air-dried (ad) poly(styrene butyl acrylate lacrylic acid) latexes and nanocomposites.

Scanning Electron Microscopy (SEM)

Microscopy and microchemical analyses were done on a JEOL JSM-6360 LV scanning electron microscope, using Secondary Electron Imaging (SEI) and Backscattering Electron Imaging (BEI). Energy Dispersive X-Ray Analysis (EDX) was done in the same microscope with a Noran System Six microanalysis system. A Supra 55VP ZEISS field emission SEM was also used. Monolith sections were cut at room temperature using a razor blade, placed on a carbon sample holder and coated with a thin carbon layer, using a MED 020 Sputter (BalTech).

Average pore size and surface area

At least 9 features (pore size, lamellar spacing and/or lamellar thickness) were measured from SEM micrographs using the Image Pro Plus 4.0 software. Average pore size and surface area were also determined from nitrogen adsorption in an ASAP 2010 apparatus from Micromeritics.

Density and porosity

The apparent density and porosity of dry monoliths were calculated using a pycnometer and distilled water as the immersion fluid. Samples between 0.4 - 0.65 mm^3 were weighed in an analytical balance (Mars-220 AM; d=0.0001g) and immersed at room temperature in a weighed 50 mL pycnometer pre-filled with water. Assays were performed in triplicate for

each sample.

Adsorption tests

Ca. 0.15 g of each freeze-cast adsorbent was added to 4 mL of 300 mg/L MB aqueous solution and left under constant stirring by inversion (18 rpm), at 25 °C for 1 h. The same procedure was repeated using 0.009 g clay as adsorbent, but in this case, the flasks were centrifuged for 10 min at 2500 rpm, in order to separate clay particles from supernatant after contact. The supernatant absorbance, at 665 nm was measured in a UV–Vis spectrophotometer (Pharmacia). Triplicate assays were made for each sample.

Compression tests

Cylindrical specimens (Ø ≈ 5.5 mm and thickness between 4 and 5 mm) were subjected to uniaxial compression under 1- 400g weights. The load was gradually increased until the specimens collapsed and the resulting deformation was measured with a digital Mitutoyo micrometer. The compressive modulus was calculated from the linear elastic range (strain < 15%) of the stress–strain curve. The comparison of stress values is presented at 50% strain. Assays were performed in triplicate for each sample.

Results and discussion

General features of samples

The freeze-cast monoliths have similar aspect (Fig. 2a), they are easy to handle but they undergo permanent deformation by compression. Reflectance (1-Transmittance) values of the samples were 0.98 for the freeze-cast monolith and 0.43 for an air dried sample with same weight per unit area. Opacity is due to light scattering by the air-filled pores. As expected, the non-porous polymer film (Fig. 2b) is translucent.

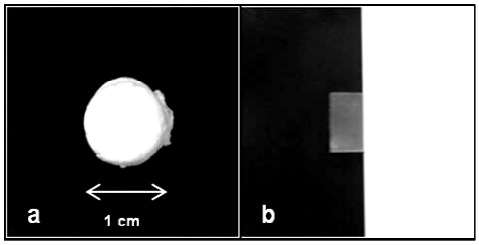

Fig. 2. Picture of poly(styrene butyl acrylate acrylic acid) monolith and film obtained respectively by (a) freeze-casting and (b) drying at 60 °C. In b) the polymer film is deposited on black and white card.

Fishbone morphology development

SEI micrograph of cut surfaces freeze-cast latex shows a complex dendritic/fishbone morphology (Fig. 3a) of oriented anisotropic pores which is unusual in amorphous polymers although it resembles "shish-kebab" structures found in semi-crystalline polymers.[41,42] This morphology is observed throughout the monoliths meaning that dendritic ice crystals are easily grown and do not stop growing until the limits of the glass mold are reached, characterizing a steady state growth.[24,43]

Fishbone morphology is unprecedented in freeze-cast monoliths prepared from common amorphous polymers in aqueous media but similar structures were obtained using more complex systems: quasiternary polyethylene/hexamethylbenzene/ /adamantine eutectic[44] and also isotactic polypropylene and pentaerythrityl tetrabromide eutectic,[45] 1,2,3,4,6-pentaacetyl β-D-galactose (BGAL) dissolved in liquid carbon dioxide,[46] porous silicon carbide (SiC) ceramics produced by freeze-casting polycarbosilane/camphene solution[47] and poly (L-lactic-co-glycolic acid) scaffolds prepared by using 1,4-dioxane as solvent.[23]

BEI micrograph (Fig. 3b) shows lamellar morphology with fishbone structures on their faces and rather uniform gray tone, evidencing low component segregation, during the formation of this elaborate morphology. Based on these micrographs we can infer that during sample freezing, lamellar ice crystals grow along the temperature gradient while smaller side branches grow at an angle. The formation of dendrites on lamellar ice crystals occurs under very high cooling rates and results from the balance between two directions of ice crystal growth: one parallel to the temperature gradient and another along the preferred direction of crystal growth, determined by interfacial energies.[24]

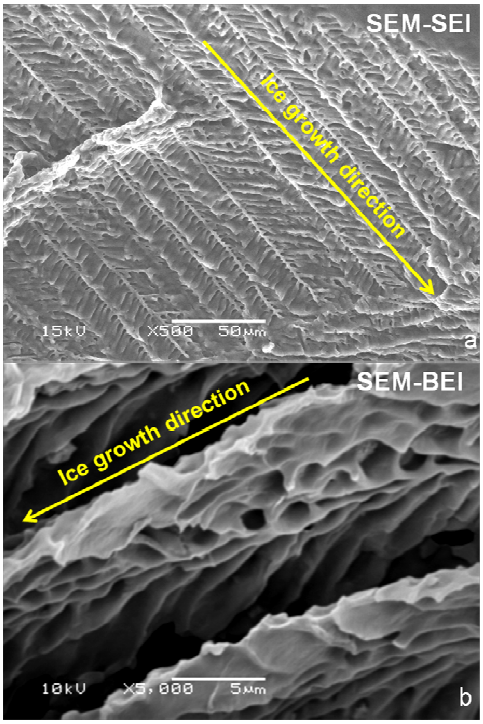

Fig. 3. Anisotropy in freeze-cast poly(styrene butyl acrylate acrylic acid) latex: (a) SEI and (b) BEI micrographs showing cross-sections parallel and perpendicular to the ice front, respectively. Homogeneous chemical composition is evidenced in BEI micrograph.

Morphological transitions

In addition to fishbone morphology, freeze-cast latex shows a variety of pore morphologies templated by different ice crystal habits (planar, columnar, lamellar) formed by time-dependent crystal transitions, as previously reported for directional freeze-casting in ceramic and polymer materials.[18,24,43,48-51] Such transitions of ice were clearly evidenced observing SEM images of freeze-cast hydroxyapatite[43] and alumina suspension,[24] and can be triggered by a Mullins-Serkerka instability.[52] Other instabilities related to the size and concentration of particles, in

addition to solidification kinetics may also influence that process, but it is not clear at this point which of these mechanisms is dominating.[18,24]

A representation of the morphological transitions of the ice crystal is shown in Fig. 4. Three distinctly different ice structures are formed due to different temperature gradients at different locations within the sample, following previous reports.[24,43,53,54] According to this mechanism, as the ice front advances, the temperature gradient is reduced and ice crystals undergo transitions that are time-dependent and which are spatially registered in the sample.[18,21,24,43]

Initial stages of sample freezing close to the container walls produces particles entrapped at the first frozen zone. Then, the interface moves progressively forming columnar and lamellar ice structures, excluding particles and yielding elongated and layered pores, respectively.[18,43] This is also observed in the present work. Cellular pore morphology (Fig. 5) is observed near to the glass wall while elongated pore morphology (Fig. 6a) is observed up to 2 mm away from it.

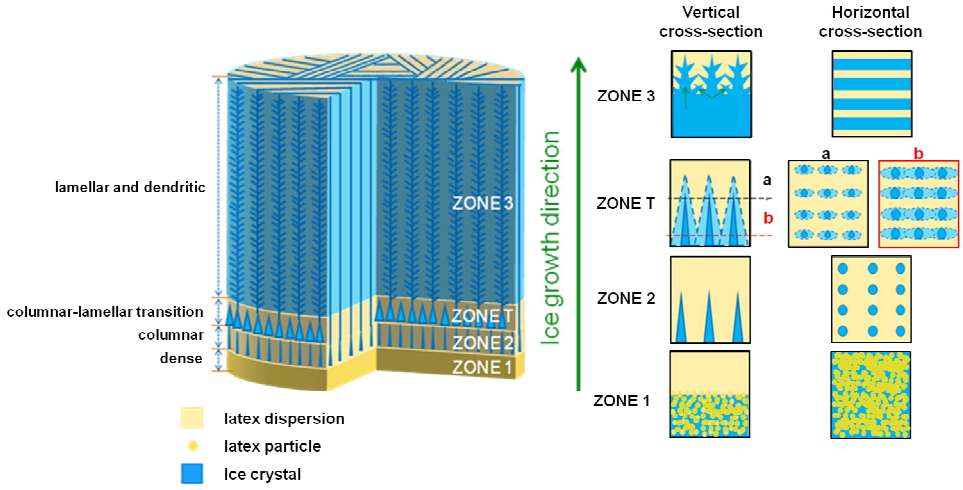

Fig. 4. Scheme of morphology changes during latex freezing.

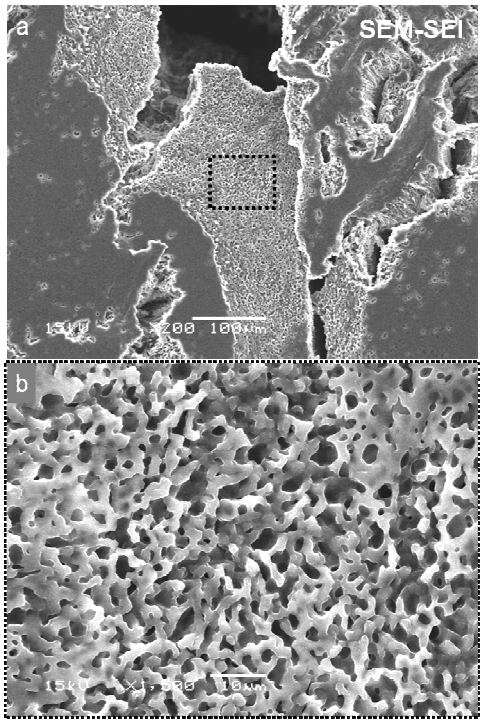

Fig. 5. SEI micrographs of freeze-cast poly(styrene-butyl acrylate-acrylic acid) show (a) flat wall formed in contact with the container walls and cellular pores and (b) magnification of cellular pores of the region outlined in black in a).

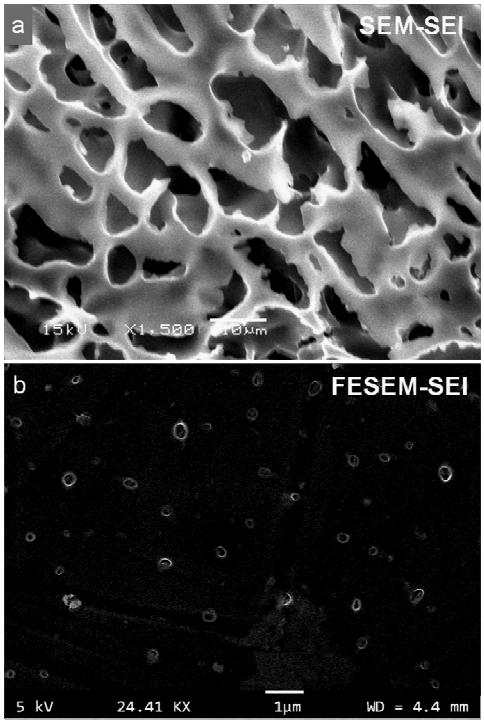

Fig. 6. SEI micrographs show (a) elongated pores of freeze-cast poly(styrene butyl acrylate acrylic acid) latex and (b) detail of the same latex dried under air.

Subsequently, morphological sidebranching instability takes place substituting lamellar pores for a dendritic shape.[24,55] This transition occurs under very high cooling rates and it results from the balance between two directions of ice crystal growth: one parallel to the temperature gradient and another along the preferred direction of crystal growth, determined by interfacial energies.[24] Thus, the morphological diversity observed in this work is explained as the result of ice crystallization under different temperatures and temperature gradients, depending on the distance from the container walls. The same latex dried at 60 °C imaged under higher magnification (Fig. 6b) presents fewer pores on its surface (probably templated by air bubbles), with 0.24± 0.05 μm average diameter and thus much smaller than the pores obtained by freeze-casting.

Morphology after clay addition

Clay introduces significant changes in pore morphology with the prevalence of lamellar architecture (Fig. 7a) carrying small pores (Fig. 7b and 7c) and absence of fishbone morphology.Surface area is about 80 ± 20 times higher while the average pore size is 1/140 that of plain polymer (Table 1). On the other hand, foamed samples do not show significant change in surface area due to clay addition.

Differences between average pore sizes determined from BET and SEM micrographs (Table 1) also indicate the existence of a second level porosity in non-foamed samples, as recently observed in a work of Hunger and co-workers,[56] in which BET measurements confirmed the existence of nanoporosity indicated in SEM micrographs of freeze-cast chitosan/gelatin/alumina composites.

Similar lamellar structures were obtained in porous alumina ceramics freeze-cast from aqueous dispersion.[24] The authors assigned it to homogeneous ice nucleation coupled to particle exclusion by the advancing solidification front forming lamellar or columnar ice morphology, while roughness on the walls was assigned to ceramic particles trapped in between the ice dendrites.[24] In two other publications, separate parallel lamellae were also observed in the microstructure of freeze-cast glycerol-plasticized casein scaffolds with and without clay, respectively.[36,57]

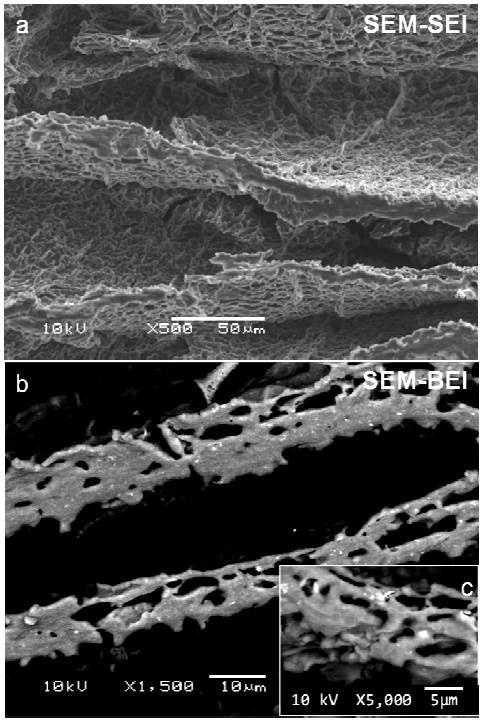

Fig. 7. SEI and BEI micrographs of freeze-cast poly(styrene-butyl acrylate-acrylic acid) with clay (6% w/w) show (a) lamellar structure, (b) pores inside lamellae and (c) detail evidencing chemical segregation by BEI contrast.

When a polymer-clay nanocomposite is dried under air, lamellae of clay tend to align parallel to each other, creating extensive domains stabilized by electrostatic adhesion.[33,58] Transmission Electron Microscopy (TEM) pictures of both poly(styrene-co-butyl acrylate-co-acrylic acid) latex and natural rubber and its clay nanocomposites were previously published by this group and show exfoliated clay lamellae together with some very small tactoids, for both polymers. TEM micrographs never show void

Table 1. Structural properties of freeze-cast samples.

Sample	Morphology	SEM micrographs				*BET analysis*	
		Lamellae spacing (μm)	Lamellae thickness (μm)	Average pore size (μm) Width	Length	Surface area (m^2g^{-1})	Average pore size (nm)
latex	cellular	-	-	2.7 ± 1.2 (100)		$0.5_1 \pm 0.2_1$ (2)	331.0 ± 5.0 (2)
	elongated	-	-	7.3 ± 3.9 (36)			
	lamellar	7.0 ± 1.1 (19)	2.5 ± 0.7 (19)	-	-		
	fishbone	-	-	$3.0 \pm 0.7_6$ (84)	8.2 ± 3.1 (75)		
latex + NaMMT	lamellar	67.4 ± 1.5 (9)	13.2 ± 1.6 (10)	-	-	39.1*	2.4*
	roughness	-	-	4.3 ± 1.6 (20)	7.0 ± 3.5 (20)		
foamed latex	cavities	-	-	$(6.5 \pm 1.6).10$ (20)		5.1*	**
	fishbone	-	-	$2.0 \pm 0.2_9$ (17)	4.2 ± 1.3 (17)		
foamed latex+ NaMMT	cavities	-	-	(9.7 ± 2.8) 10 (15)		3.2*	**
	lamellar	3.8 ± 1.8 (19) ^{F} $(3.4 \pm 1.5).10$ (20) ^{L}	$2.3 \pm 0.6_5$ (11) ^{F} 9.6 ± 3.2 (17) ^{L}	-	-		

Numbers inside the parentheses indicate number of replicates.
Superscripts F and L indicate foam and liquid regions for the same sample.
- Not applicable.
* Measures without replicates.
** Not measured.

formation or ruptured film areas in the polymer–clay platelet interface, evidencing strong polymer-particle adhesion.[33,58] Clay interacts strongly through ionic bridges formed by the ions trapped between the latex particles and the clay platelets.[39] When the sample is freeze-cast, lamellar morphology prevails because clay particles line-up parallel to the ice crystal faces during freezing, from aqueous precursor dispersion with clay concentration higher than 0.7% (w/w).[29,38,59] Below this concentration, added clay was not self-assembled[59] and in our case, clay concentration (1.15% w/w) in the aqueous precursor dispersion was sufficient to produce this morphology. Furthermore, clay platelets act as barriers to propagation of ice crystals growth due to their stiffening effect and large aspect ratio.[36] Details of dendritic crystals like their fine branches are thus lost and fishbone features are not observed. The same effect on filling the otherwise interdendritic spaces was previously observed whit alumina particles of different sizes.[18,21]

Deville and co-workers also observed that the growth pattern produces roughness/dendrites on only one side of lamellae,[24] directly related to the morphology of the solvent crystal.[18] However, in the present work, roughness of freeze-cast nanocomposite (Fig. 7a) and fishbone morphology of freeze-cast latex (Fig. 3) are obtained from the same solvent and observed on both sides of lamellae.

BEI micrographs of nanocomposites (Fig. 7b, 7c and 8) show some brighter domains that correspond to areas with higher average atom number. X-ray energy-disperse spectroscopy identified carbon, oxygen, sodium, aluminum, silicon and sulfur in these spots, while the elemental maps revealed that some spots are composed predominantly of the elements oxygen, sodium and sulfur while others contain oxygen, aluminum and silicon. This information evidences that aggregates contain respectively sodium sulphate (from the latex polymerization initiator, sodium persulfate) and sodium montmorillonite.

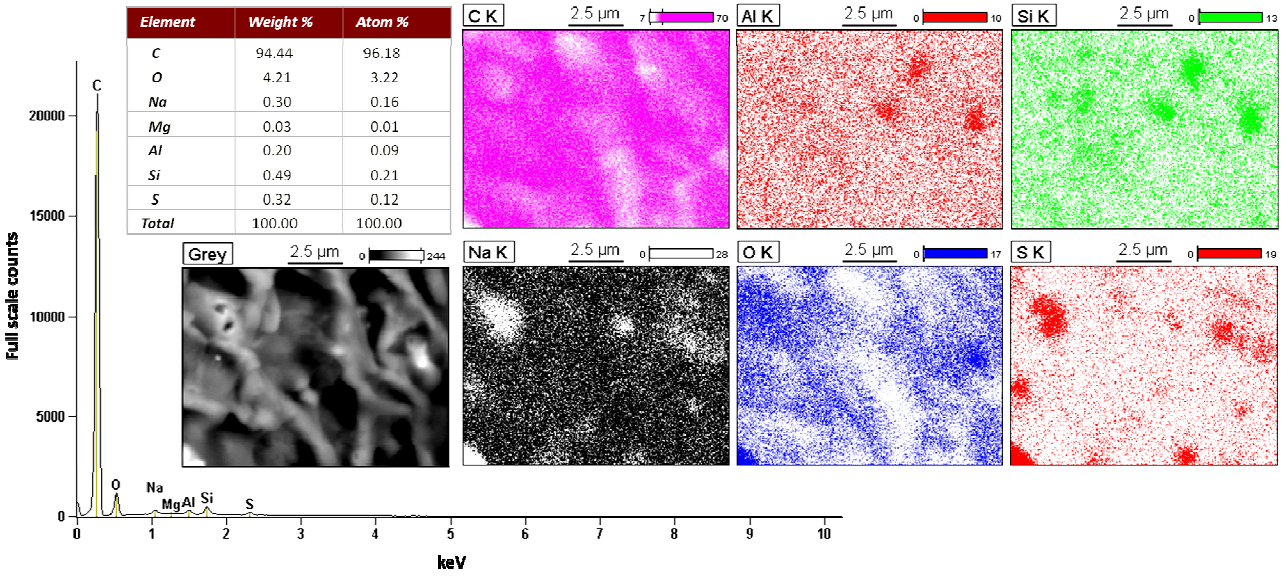

Fig. 8. X-ray spectrum, BEI micrograph and the corresponding EDX elemental distribution maps of freeze-cast poly(styrene - butyl acrylate - acrylic acid)/clay nanocomposite. Note the correspondence between bright spots in BEI image and dotted areas in elemental maps. Al and Si accumulate together, as well as Na and S.

Morphology of foamed latex

The cut surfaces of monoliths obtained from foamed latex shows interconnected spherical cavities distributed throughout (Fig. 9) containing smaller pores with fishbone morphology on their walls. The addition of the clay dispersion to the foamed latex decreases foam stability and the liquid drains faster, leaving residual foam in the top and liquid in the bottom of the glass mold.

SEM micrograph of the cut surface in Fig. 10a shows the contact area between foamed and drained liquid regions. The former (with the circled area) contains rounded structures while the latter (with a square) is similar to Fig. 6a. The cavities templated by air bubbles in Fig. 10b show smaller lamellar pores, similar to the frozen nanocomposite without foaming. Akin foam morphologies were obtained by using styrene–divinyl benzene polymer to obtain a material with 90 vol % porosity and high relative water adsorption, with potential use as soil additive in agroprocess intensification, but by using more complex procedure.[9]

Results obtained using commercial latexes

Results presented so far in this report refer to P(S-BA-AA) latex obtained in this laboratory and its nanocomposites, but both lamellar and fishbone morphologies were also obtained with two commercial styrene-acrylic latexes (Figs. 11 and 12).

Dye adsorption

Adsorbate removal by freeze-cast monoliths ranged from 3.1% (foamed latex) to 99.8% (foamed latex + NaMMT) (Fig. 13). For the sake of comparison, a nanocomposite film prepared by casting and a clay dispersion, both with the same amount of clay contained in freeze-cast nanocomposites, were used as adsorbents.

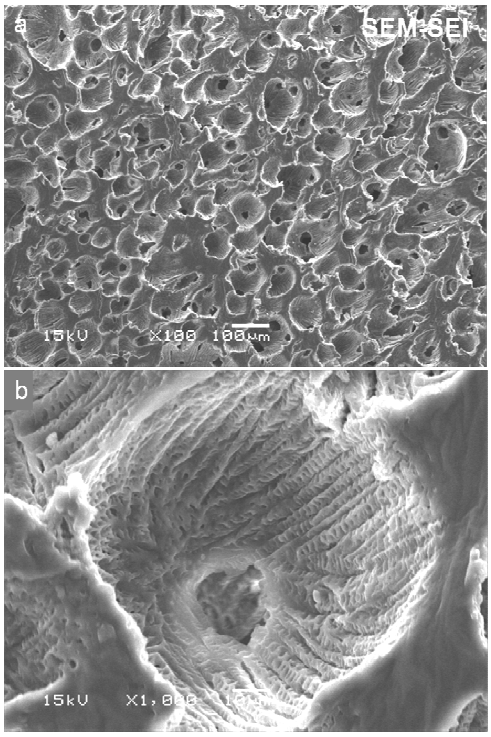

Fig. 9. SEI micrographs of freeze-cast foamed poly(styrene butyl acrylate acrylic acid) latex show (a) pore distribution and (b) interconnected pore details.

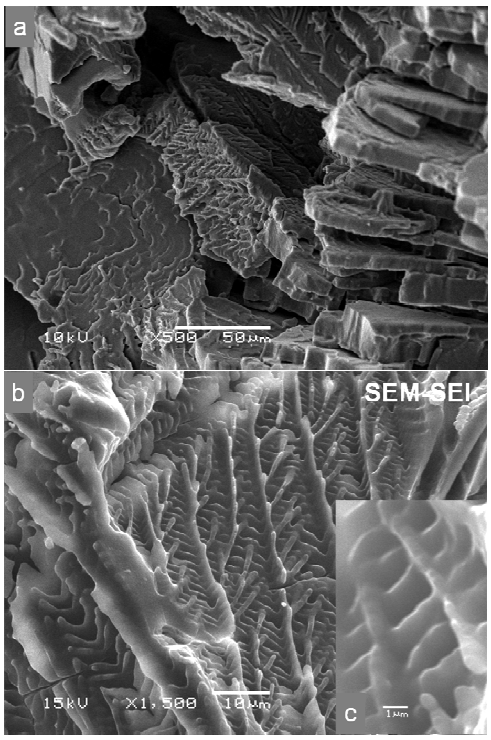

Fig. 11. SEI micrographs of freeze-cast poly(styrene butyl acrylate) from Basf show cross-sections perpendicular (a) to the ice front and parallel to the ice front (b,c).

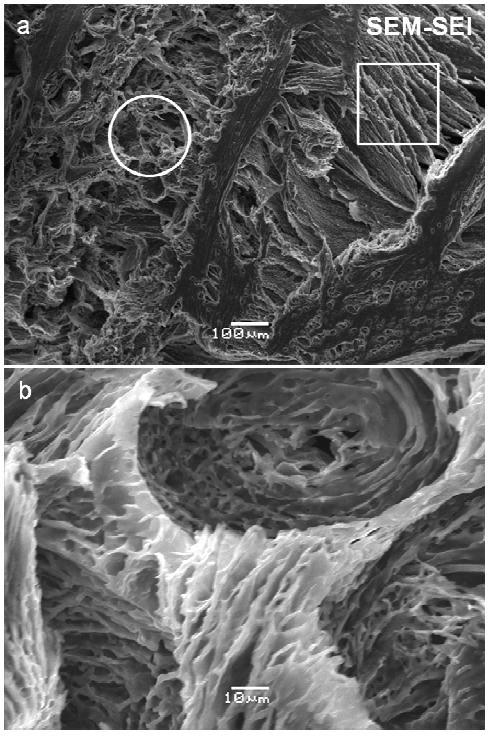

Fig.10. SEI micrographs of foamed poly(styrene-butylacrylate-acrylic acid) latex with clay (6% w/w) show (a) the interface between foam (circle) and drained liquid (square) regions of monolith and (b) detail of foamed region.

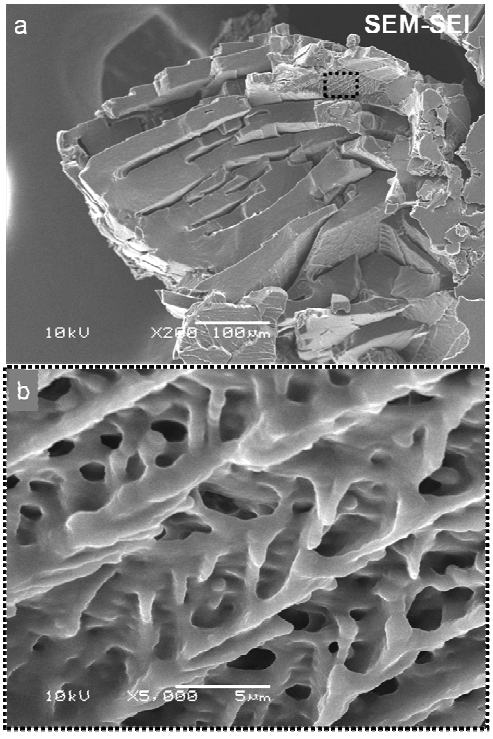

Fig. 12. SEI micrographs of freeze-cast porous poly(styrene butyl acrylate) from Denver show cross-section perpendicular to the ice front (a) and roughness detail of the region outlined in black (b).

Clays are good adsorbents because of the existence of several types of active sites on the surface, which include Brönsted and Lewis acid sites beyond ion exchange sites.[5] Latex samples with clay show almost the same capacity to adsorb dye as the clay dispersion itself, showing that the freeze-cast nanocomposites may be used as convenient, pelleted adsorbents, with great potential application in dye removal from aqueous solution (Supplementary Fig. S2 and S3).

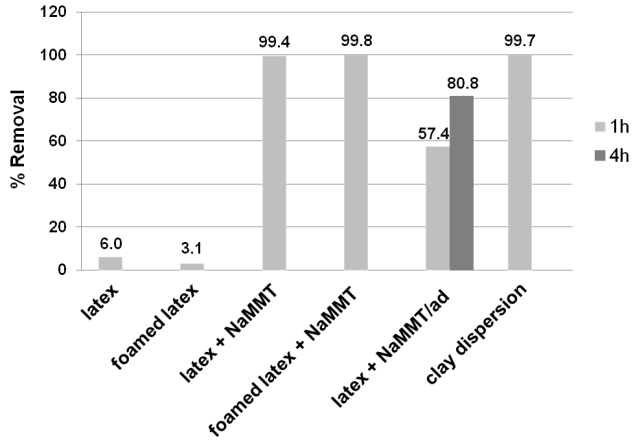

Fig. 13. Removal of aqueous methylene blue solution (300 mg/L) with time in presence of clay dispersion (2.25 mg/mL) and different freeze cast adsorbents (35 mg /mL). Air-dried sample is indicated by ad.

Mechanical strength and water stability of the monoliths can probably be improved by cross-linking, but this was not made in this work.

Dye removal using cast nanocomposite film increases from 57 % to 81 % by increasing the contact time from 1 to 4 h, while dye removal reaches 99 % using freeze-cast nanocomposites, after 1 h. According to previous publications, when a nanocomposite film is prepared by casting, positive counterions of the styrene-acrylic latex[58] or natural rubber[33] particles form ionic bridges, responsible for strong adhesion between clay and latex particles that (both) contain excess negative charges. These strongly cation binding sites account for MB adsorption.[39] Interaction between the filler and the latex matrix is electrostatic.[33,39,58,60] Since strong binding sites are formed at clay-polymer interfaces, we expect that adsorption capacity increases with filler volume fraction, This is an important question to be answered by future (and extensive) work.

Following the previous work of Braga *et al.* and our own observations in the laboratory, dye desorption from the nanocomposite is slow and incomplete.[61] Dye molecules are trapped in the clay/polymer interface benefiting from a strong electrostatic attraction and also from polymer hydrophobicity that is absent from clay-only adsorption sites.[61]

Although the removal of MB by clay dispersions[62-64] and different clay nanocomposites[2,5-7] have been previously studied, freeze-cast nanocomposites are the first examples of effective lamellar adsorbents prepared from common amorphous polymer and clay. These results reveal the large potential of freeze-casting in the field of water remediation. In structured adsorbents, lamellar structures with sufficient small spacing and width (< 0.2 mm) are promising structures with enhanced mass transfer compared to pellets, monoliths or foams with the same density.[65]

Compression tests

The compression results (Fig. 14) show an initial linear elasticity due to elastic cell wall bending when the strain is less than 15%. Increasing strain causes plastic deformation and finally, densification. These deformation steps are also observed during compression of polymeric foams[66] like epoxy,[67] foamed latex rubber[68] and cellulose nanowhisker reinforced acrylic foams made by freeze-casting.[69]

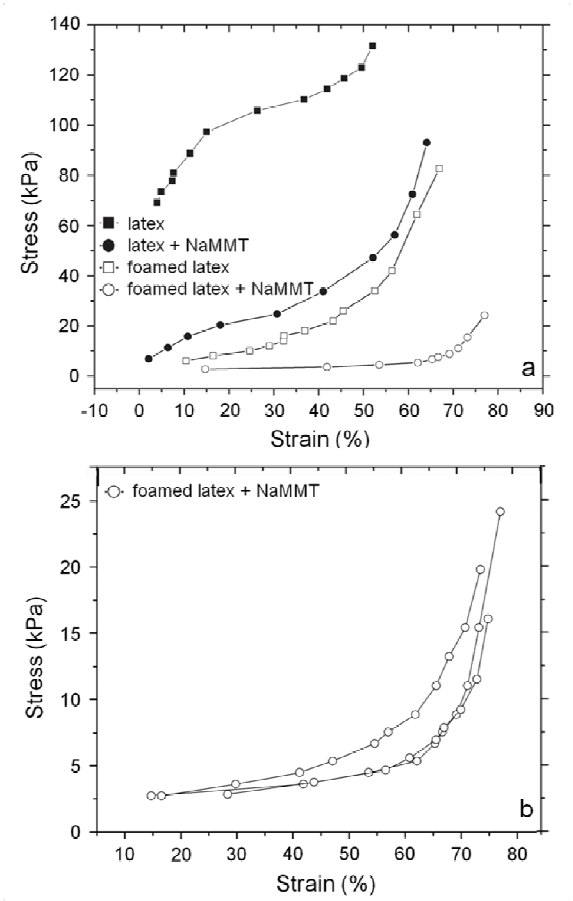

Fig. 14. a) Compressive stress–strain data for all samples and b) triplicate measurements for foamed poly(styrene - butyl acrylate - acrylic acid)/clay nanocomposite. Continuous lines are just connecting the experimental points.

Comparing nanocomposite (porosity = 79%) with foamed latex (porosity = 81%) (Table 2) we can infer that an additional improvement in compressive stress for non-foamed samples could be assigned to their anisotropic lamellar structure while foamed samples have only random isotropic cavities.

Similar behaviour was observed in a recent work by Xu and co-workers,[69] in which acrylic foams samples reinforced with cellulose nanowhiskers (CNW) were prepared by both directional and non directional freeze-casting. Improvements in mechanical properties along the loading direction of freeze-cast samples were assigned to reinforcement by CNWs added to the reduction of cell size and cell allignment.

Table 2. Density, porosity and stress–strain data for freeze-cast and air-dried samples.

Sample	Density (g cm^{-3})	Porosity (%)	Stress at 50% strain (kPa)	Compressive Modulus (kPa)
latex	0.3438 ± 0.0005	66.2 ± 0.9	119 ± 7	$23_{.4} \pm 3_{.3}$ (10)
latex + NaMMT	0.211 ± 0.003	78.5 ± 0.3	43 ± 5	85 ± 3
foamed latex	0.183 ± 0.003	81.4 ± 0.9	27 ± 4	64 ± 4
foamed latex+ NaMMT	0.101 ± 0.007	89.9 ± 0.7	5 ± 1	15 ± 4
latex/a-d [a]	≈ 1	≈ 0	*	*
latex + NaMMT/a-d [a]	≈ 1	≈ 0	*	*

a- Air-dried samples are indicated by a-d.

* Not measured

Conclusions

Freeze-cast latex and latex/clay nanocomposites are low density porous solids with various pore morphologies (fishbone, lamellar, cellular) templated by ice crystals. Fishbone complex morphology is assigned to ice crystallization along the freezing temperature gradient combined to the formation of side branches growing normal to the temperature gradient. Hierarchic solid foams carrying dendritic and lamellar pores along the walls of cavities that are in turn templated by air bubbles were also obtained. The formation of complex porous structures produces water-insoluble porous nanocomposite that can be used as an effective dye sorbent, as much as exfoliated clay in water. This is the first example of nanocomposite adsorbents prepared by freeze-casting.

Acknowledgements

L.L.S. thanks CNPq fellowship. This is a contribution from the INCT Inomat, a project supported by Brazilian agencies MCTI/CNPq and Fapesp. Thanks also go to Ziarat Shah that synthesized the P(S-BA-AA) latex.

Notes and references

[a] *Institute of Chemistry, University of Campinas, Campinas SP, Brazil 13083-862. Fax: +55 19 3521 3023; Tel.: +55 19 3521 3014; E-mail: lucimarals@yahoo.com.br, fernagal@iqm.unicamp.br.*

[b] *National Nanotechnology Laboratory @ National Center for Energy and Materials Research, Campinas SP, Brazil 13083-97. Fax: +55 19 3212 1004; Tel. +55 19 3518 3103; E-mail: fernando.galembeck@lnnano.cnpem.br.*

† Electronic Supplementary Information (ESI) available: (1) Description and picture of home-made apparatus; (2) Pictures showing water resistance and no significant dimensional changes before and after two years water immersion; (3) Plotting showing water sorption by freeze-cast foamed latex and nanocomposite monoliths. See DOI: 10.1039/b000000x/

1) Description of home-made apparatus.

The home-made freeze-dryer (Fig. S1a) was attached to a glass chamber coated with a thermal blanket (Fig. S1b) and connected to a vacuum pump in order to improve the thermal insulation. That chamber contains therein a reservoir of liquid nitrogen to keep the round bottom glass flasks chilled during lyophilization. The pressure (90 mmHg) and temperature were measured using a vacuum gauge and a thermocouple of contact, respectively. Fig. S1c shows a crust of snow formed on the outside of a round bottom flask. After flasks reached room temperature, the samples were kept in the freeze-dryer for a further hour to ensure that were dry. Ice melting was not observed during freeze-drying.

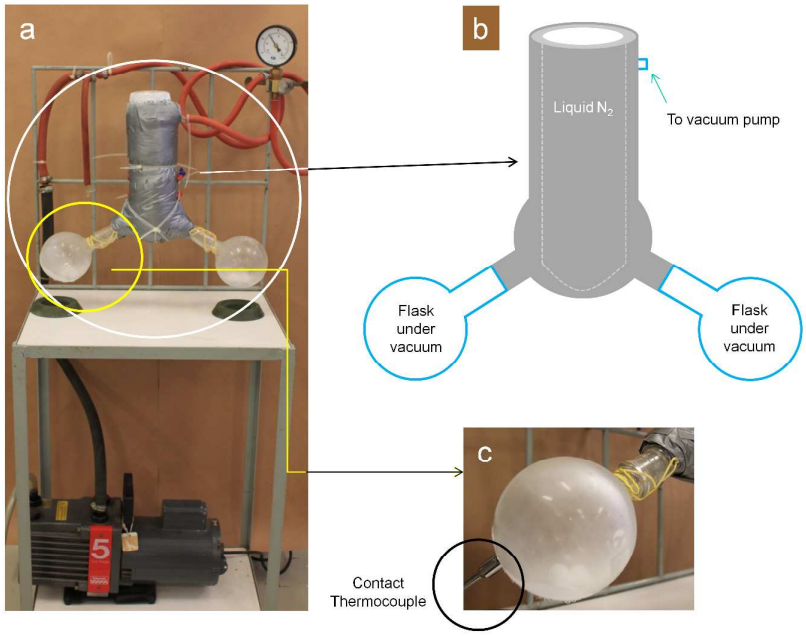

Fig. S1: Picture of home-made apparatus used in freeze-drying (a), schematic drawing showing the vacuum chamber and its interior (b) and detail of a round bottom glass flask under vacuum and a contact thermocouple (c).

2) Resistance to water tests

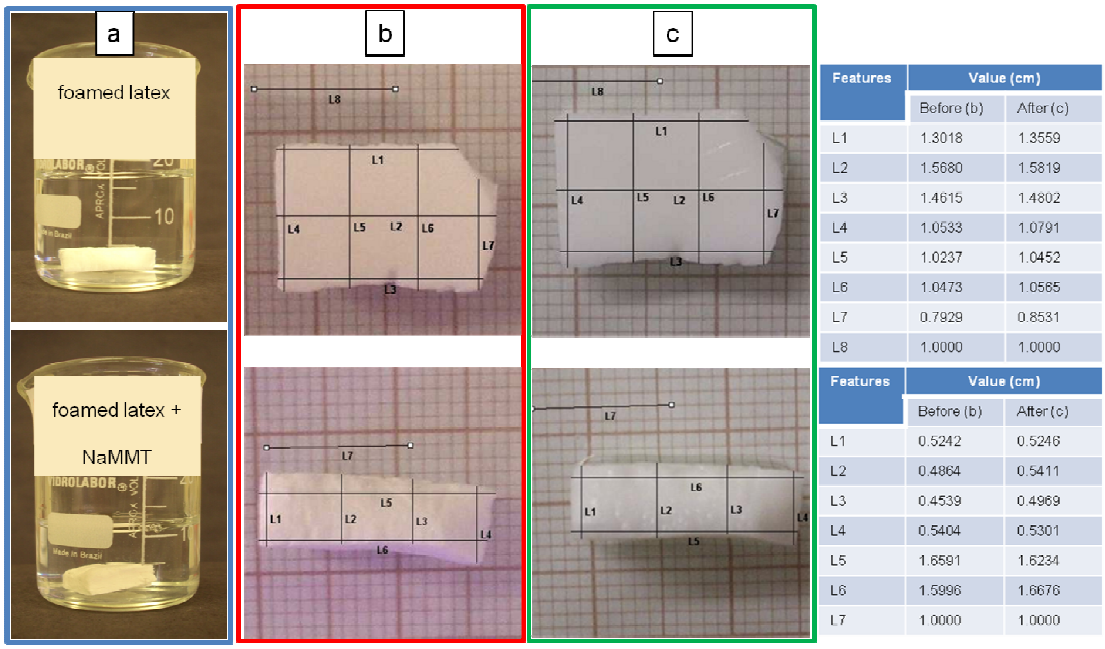

Features	Value (cm)	
	Before (b)	After (c)
L1	1.3018	1.3559
L2	1.5680	1.5819
L3	1.4615	1.4802
L4	1.0533	1.0791
L5	1.0237	1.0452
L6	1.0473	1.0585
L7	0.7929	0.8531
L8	1.0000	1.0000

Features	Value (cm)	
	Before (b)	After (c)
L1	0.5242	0.5246
L2	0.4864	0.5411
L3	0.4539	0.4969
L4	0.5404	0.5301
L5	1.6591	1.6234
L6	1.5996	1.6676
L7	1.0000	1.0000

Fig. S2. Pictures of freeze-cast foamed poly(styrene butyl acrylate acrylic acid) latex and nanocomposite monoliths immersed in deionized water for two years (a) and pictures of freeze-cast foamed latex monolith showing no significant dimensional changes before (b) and after two years (c) water immersion. The other freeze-cast samples showed similar behavior.

3) Water sorption

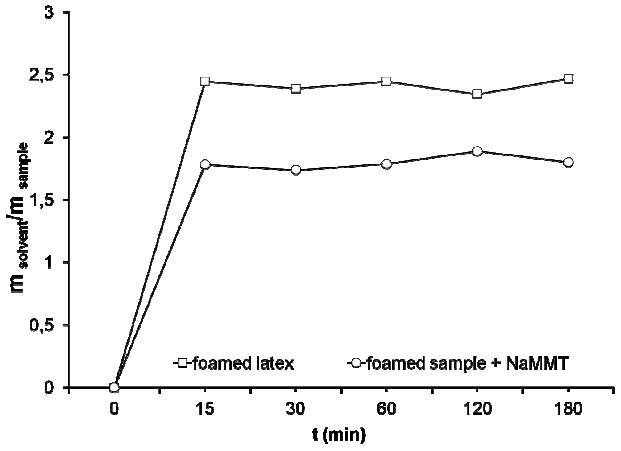

Fig. S3. Water sorption by freeze-cast foamed poly(styrene butyl acrylate acrylic acid) latex and nanocomposite monoliths.

1 L. Jin, Q. Liu, Y. Yang, H. Fu and W. Sun, *J. Colloid. Interf. Sci.*, 2014, **426**, 1-8.
2 L. Ai, Y. Zhou and J. Jiang, *Desalination*, 2011, **266**, 72-77.
3 Y. Li, Q. Dua, T. Liua, X. Peng, J. Wang, J. Suna, Y. Wang, S. Wua, Z. Wang, Y. Xia and L Xia, *Chem. Eng. Res. Des.*, 2013, **9(1)**,361-368.
4 Q. Zheng, Z. Cai and S. Gong, *J. Mater. Chem. A,* 2014, **2**, 3110-3118.
5 R. Srinivasan, *Adv. Mater. Sci. Eng.,* 2011, **2011**, ID 872531;doi:10.1155/2011/872531.
6 E. Gunister, A. M. Bozkurt and H. Catalgil-Giz, *J. Appl. Polym. Sci.,* 2013, **129(3)**, 1232-1237.
7 S. R. Shirsath, A. P. Patil, R. Patil, J. B. Naik, P. R. Gogate and S. H. Sonawane, *Ultrason. Sonochem.,* 2013, **20**, 914.
8 S. Wang, R. Castro, X. An, C. Song, Y. Luo, M. Shen, H. Tomás, M. Zhub and X. Shi, *J. Mater. Chem.,* 2012, **22**, 23357-23367.
9 D. R. Burke, G. Akay and P. E. Bilsborrow, *J. Appl. Polym. Sci.,* 2010, **118**, 3292-3299.
10 X. Guo, Z. Zhou, S. Wang, S. Zhao, Q. Zhang and G Ma, *J. Porous Mater.,* 2012, **19**, 853-858.
11 F. Dehghani and N. Annabi, *Current Opinion in Biotech*., 2011, **22**, 661-666.
12 C. Ji, N. Annabi, A. Khademhosseini and F Dehghani, *Acta Biomater.,* 2011, **7(4)**, 1653-1664.
13 J. H. Pan, H. Dou, Z. Xiong, C. Xu, J. Ma and X. S. Zhao, *J. Mater. Chem.*, 2010, **20**, 4512-4528.
14 S. Hong, J. H. Moon, J. Lim, S. Kim and S. Yang, *Langmuir*, 2005, **21**, 10416-10421.
15 D. Chen, X. Wang, T. Liu, X. Wang and J. Li, *ACS Appl. Mater. Interfaces,* 2010, **2(7)**, 2005-2011.
16 Y. Sun, H. Cui, S. X. Jina and C. X. Wang, *J. Mater. Chem*., 2012, **22**, 16566-16571.
17 Y. Zhang, L. Hu, J. Han, Z. Jiang, *Ceram. Int.,* 2010, **36**, 617-621.
18 S. Deville, *Adv. Eng. Mater.,* 2008, **10**, 155-169.
19 M. Barrow, A. Eltmimi, A. Ahmed, P. Myers and H. Zhang, *J. Mater. Chem.*, 2012, **22**, 11615-11620.
20 C. Gaudillere, J. Garcia-Fayos and J. M. Serra, *J. Mater. Chem. A*, 2014, **2**, 3828-3833.
21 S. Deville, E. Saiz, R. K. Nalla and A. P. Tomsia, *Science,* 2006, **311(27)**, 515-518.
22 C. M. Pekor, B. Groth and I. Nettleship, *J. Am. Ceram. Soc.,* 2010, **93(1)**, 115-120.
23 F. Yang, X. Qu, W. Cui, J. Bei, F. Yu, S, Lu and S. Wang, *Biomaterials*, 2006, **27**, 4923-4933.
24 S. Deville, E. Saiz and A. P. Tomsia, *Acta Mater*., 2007, **55(6)**, 1965-1974.
25 C. T. McKee and J. Y. Walz, *J. Am. Ceram. Soc.,* 2009, **92(4)**, 916-921.
26 H. J. Choi, T. Y. Yang, S. Y. Yoon, B. K. Kim and H. C. Park, *Mater. Chem. Phys.*, 2012, **133**, 16-20.
27 Y. H. Koh, E. J. Lee, B. H. Yoon, J. H. Song and H. E. Kim, *J. Am. Ceram. Soc.,* 2006, **89(12)**, 3646-3653.
28 U. G. K. Wegst, M. Schecter, A. E. Donius and P. M. Hunger, *Philos. Trans. R. Soc. A*, 2010, **368**, 2099-2121.
29 T. Pojanavaraphan, D. A. Schiraldi and R. Magaraphan, *Appl. Clay Sci.,* 2010, **50**, 271-279.
30 M. D. Gawryla, M. Nezamzadeh and D. A. Schiraldi, *Green Chem*., 2008, **10**, 1078-1081
31 A. Ojuva, F. Akhtar, A. P. Tomsia and L. Bergström, *ACS Appl. Mater. Interfaces,* 2013, **5**, 2669-2676.
32 H. Mori, K. Aotani, N. Sano and H. Tamon, *J. Mater. Chem.,* 2011, **21**, 5677.
33 L. F. Valadares, C. A. P. Leite and F. Galembeck, *Polymer*, 2006, **47**, 672-678.
34 M. S. Hassan and K. F. El-Nemr, *J. Ind. Eng. Chem.,* 2013, **19**, 1371-1376.
35 M. D. Gawryla and D. A. Schiraldi, *Macromol. Mater. Eng.,* 2009, **294(9)**, 570-574.
36 T. Pojanavaraphan, R. Magaraphan, B. Chiou and D. A. Schiraldi, *Biomacromolecules*, 2010, **11**, 2640-2646.
37 T. Pojanavaraphan, L. Lei, C. Deniz, O. Oguz, R. Magaraphan and D. A. Schiraldi, *Macromolecules,* 2011, **44**, 923-931.
38 T. Pojanavaraphan and R. Magaraphan, *Eur. Polym. J.,* 2008, **44**, 1968-1977.
39 L. F. Valadares, E. M. Linares, F. C. Bragança and F. Galembeck, *J. Phys. Chem. C*, 2008, *112*, 8534-8544.
40 A. J. Keslarek, C. A. R. Costa and F. Galembeck, *Langmuir,* 2001, **17**, 7886-7892.
41 M. van Heeringen, B. Vastenhout, R. Koopmans and L. Aerts, *e-Polymers,* 2005, **48**, ISSN 1618-7229.
42 J. F. Mano, R. A. Sousa, R. L. Reis, A. M. Cunha and M. J. Bevis, *Polymer*, 2001, **42(14)**, 6187-6198.
43 S. Deville, E. Saiz and A. P. Tomsia, *Biomaterials*, 2006, **27**, 5480-5489.
44 P. Smith, R. Konigsveld, C. J. H. Schouteten and A. J. Pennings, *Brit. Polym. J.*, 1980, **12**, 215-220.
45 P. Smith and A. J. Pennings, *J. Polym. Sci. B Polym. Phys. Edition*, 1977, **15**, 523-540.
46 H. Zhang, J. Long and A. I. Cooper, *J. Am. Chem. Soc.,* 2005, **127**, 13482-13483.
47 B. H. Yoon, E. J. Lee and H. E. Kim, *J. Am. Ceram. Soc.,* 2007, **90(6)**, 1753-1759.
48 T. Moritz and H. Richter, *J. Amer. Ceram. Soc.,* 2006, **89(8)**, 2394-2398.
49 A. Preiss, B. Su, S. Collins and D. Simpson, *J. Eur. Ceram. Soc.,* 2012, **32**, 1575-1583.
50 S. V. Madihally and H. W. T. Matthew, *Biomaterials*, 1999, **20(12)**, 1133-1142.
51 S. Zmora, R. Glicklis and S. Cohen, *Biomaterials*, 2002, **23(20)**, 4087-4094.
52 W. W. Mullins and R. F. Sekerka, *J. Appl. Phys.,* 1963, **34(2)**, 323-329.
53 M. A. Azouni, P. Casses, B Sergiani. *Colloids Surf A.*, 1997, **122(1-3)**,199-205.
54 Y. Chino, D. C. Dunand. *Acta Mater*., 2008, **56(1),**105-113.
55 D. T. J. Hurle, in Crystal Growth Handbook, ed. Elsevier, Amsterdam, vol. 2, pp. 1993-1994.
56 P. M. Hunger, A. E. Donius and U. G. K. Wegst *Acta Biomater.,* 2013, **9**, 6338–6348.
57 A. Ghosh, M. A. Ali and G. J. Dias, *Biomacromolecules*, 2009, **10(7)**, 1681-1688.
58 F. C. Bragança, L. F. Valadares, C. A. P. Leite and F. Galembeck, *Chem. Mater.,* 2007, **19**, 3334-3342.
59 L. S. Somlai, S. A. Bandi, D. A. Schiraldi and L. J. Mathias, *Aiche J*., 2006, **52(3)**, 1162-1168.
60 E. M. Linares, M. M. Rippel, F. Galembeck, *ACS Applied Materials & Interfaces*, 2010, 2 (12), 3648-3653.
61 M. Braga, C. A. P. Leite, F. Galembeck, *Langmuir*, 2003, 19 (18), 7580-7586

62 C. A. P. Almeida, N. A. Debacher, A. J. Downsc, L. Cotteta and C. A. D. Mello, *J. Colloid Interf. Sci.,* 2009, **332**, 46–53.
63 F. G. E. Nogueira, J. H. Lopes, A. C. Silva, M. Gonçalves, A. S. Anastácio, K. Sapag and L. C. A. Oliveira, *Appl. Clay Sci.,* 2009, **43**, 190-195.
64 F. Gessner, C. C. Schimitt and M. G. Neumann, *Langmuir*, 1994, **10**, 3749.
65 F. Rezaei and P. Webley, *Chem. Engineer. Sci.,* 2009, **64**, 5182-5191.
66 S. Ouelleta, D. Croninb and M. Worswick, *Polym. Testing,* 2006, **25**, 731-743.
67 Y. Dong, J. Dong, J. Wang, X. Fu, H. Hu, S. Li, H. Yang, C. Xu, M. Du and Y. Fu, *Compos. Sci. Technol.,* 2013, **76**, 8-13.
68 D. Klempner and K. C. Frisch, in Handbook of Polymeric Foams and Foam Technology, ed. Carl Hanser Verlag, Munich, Vienna, New York, Barcelona, 1991.
69 Z. Xu, Q. Sun, F. Huang, Y. Pu, S. Panb and A. J. Ragauskas, *RSC Adv.*, 2014, **4**, 12148.

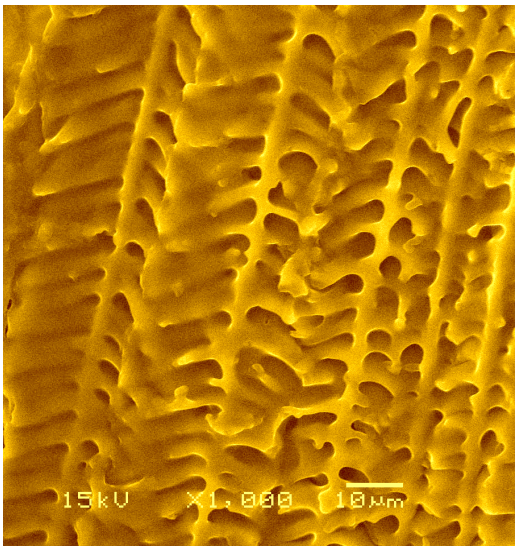

Freeze-cast monoliths prepared from common amorphous latex in aqueous media presented unprecedented morphologies that contribute to dye sorbent capacity.